ARTICLE

Reusable and highly sensitive SERS immunoassay utilizing gold nanostars and a cellulose hydrogel-based platform

Received 00th January 20xx,
Accepted 00th January 20xx

DOI: 10.1039/x0xx00000x

Maria João Oliveira[a,b], Inês Cunha[a], Miguel P. de Almeida[c], Tomás Calmeiro[a], Elvira Fortunato[a], Rodrigo Martins[a], Luís Pereira[a,d], Hugh J. Byrne[e], Eulália Pereira[c], Hugo Águas[a,*], and Ricardo Franco[b,*]

The development of robust and sensitive point-of-care testing platforms is necessary to improve patient care and outcomes. Surface-Enhanced Raman Scattering (SERS)-based immunosensors are especially suited for this purpose. Here, we present a highly sensitive and selective SERS immunoassay, demonstrated for the example of Horseradish Peroxidase (HRP) detection, in a sandwich format. The strength of our biosensor lies in merging: (i) SERS-immunotags based on gold nanostars, allowing exceptional intense SERS from attached Raman probes, covalent attachment of anti-HRP antibodies by a simple chemical method providing exceptional antigen binding activity; (ii) the ease of preparation of the capture platform from regenerated cellulose-based hydrogel, a transparent material with low background fluorescence and Raman signal, particularly suited for preserving high activity of covalently bound anti-HRP antibodies. The sandwich complexes formed were characterised by Atomic Force Microscopy, and by Scanning Electron Microscopy coupled with Electron Diffraction Spectroscopy; (iii) the robustness of the simple Classical Least Squares method for SERS data analysis, resulting in superior discrimination of SERS signals from the background and much better data fitting, compared to the commonly used peak integral method. Our SERS immunoassay greatly improves the detection limits of traditional enzyme-linked immunosorbent assay approaches, and its performance is better or comparable to existing SERS-based immunosensors. Our approach successfully overcomes the main challenges for application at point-of-care, including increasing reproducibility, sensitivity, and specificity, associated with an environmentally friendly and robust design. Also, the proposed design withstands several cycles of regeneration, a feature absent from paper-SERS immunoassays and that opens the way for sensitive multiplexing applications on a microfluidics platform.

Introduction

The relevance of biosensors that are both highly sensitive and specific, with easy translation into portable health applications, has been particularly highlighted by the need for rapid screening of large populations during the SARS-CoV-2 pandemic[1]. Surface-Enhanced Raman Scattering (SERS)-based immunosensors are especially suited to fulfil the criteria of highly sensitive and specific analyte detection, with easy adaptation to a variety of point-of-care testing (POCT) formats. Examples include lateral flow[2,3], magnetic beads[4,5], and microfluidic devices[6,7].

In a traditional SERS-immunometric assay, the analyte is sandwiched between the capture antibody and the labelled antibody. The capture antibody is immobilised on a substrate, whereas the "top bread slice" of the sandwich consists of the same antibody attached to a plasmonic metal nanoparticle (NP) labelled with a Raman probe (the SERS-immunotag)[2,8–10]. This design offers a more sensitive and versatile option for biosensing than label-free strategies[11], with easy adaptation to a microfluidics setup.

Challenges to overcome for POCT application of SERS-immunosensors are; low reproducibility, inherent to SERS-based detection methods; reduction of costs of the device, including use of low reagent and sample volumes; and easy operation and readout. Additional desirable features for the POCT assay are high sensitivity and specificity, rapidity and robustness, and an environmentally friendly design, with a view towards disposability[12]. For POCT applications, a microfluidic platform exhibits numerous advantages, including rapid response, low sample consumption, high-throughput screening ability, and portability. The high surface-to-volume ratio of micro-meter-sized channels of microfluidic devices increases reaction rates of immunoassays compared to those on solid

[a] CENIMAT-i3N, Departamento de Ciência dos Materiais, Faculdade de Ciências e Tecnologia, FCT, Universidade Nova de Lisboa, 2829-516 Caparica, Portugal; i.cunha@campus.fct.unl.pt (I.C); t.calmeiro@campus.fct.unl.pt (T.R.C.); emf@fct.unl.pt (E.F.); rfpm@fct.unl.pt (R.M.)
[b] UCIBIO, REQUIMTE, Departamento de Química, Faculdade de Ciências e Tecnologia, Universidade NOVA de Lisboa, 2829-516 Caparica, Portugal; mj.oliveira@campus.fct.unl.pt (M.J.O.)
[c] REQUIMTE/LAQV, Departamento de Química e Bioquímica, Faculdade de Ciências da Universidade do Porto, 4169-007 Porto, Portugal; mpda@fc.up.pt (M.P. de A.); eulalia.pereira@fc.up.pt (E.P.)
[d] AlmaScience, Campus da Caparica, 2829-516 Caparica (Portugal) (lmnp@fct.unl.pt)
[e] FOCAS Research Institute, Technological University Dublin, Camden Street, Dublin 8, Ireland. Hugh.Byrne@tudublin.ie (H.J.B.)
* Correspondence: hma@fct.unl.pt (H.A.); ricardo.franco@fct.unl.pt (R.F.)
Electronic Supplementary Information (ESI) available: [details of any supplementary information available should be included here]. See DOI: 10.1039/x0xx00000x

substrates or in the aqueous phase[8,13]. In addition, the continuous flow environment helps to reduce nonspecific adsorption of SERS nanoprobes, which in turn increases the sensitivity and accuracy for a quantitative detection[7].

In a SERS-immunosensor based on the sandwich design, sensitivity and selectivity improvements can be brought by the SERS-immunotag. This should present an optimal loading of antibodies that are active for antigen capture, making antibody functionalisation of the NPs a key step in the preparation of SERS-immunotags[14,15]. Antibody-orientation strategies at the surface of the NPs have been developed[16,17], but are expensive and laborious. Another necessary improvement of the SERS-immunotag lies in maximizing the detected signal and thus the biosensor sensitivity. Multibranched metal NPs, such as gold nanostars (AuNSs), show remarkable SERS performance due to their large number of intrinsic hotspots and high surface-to-volume ratio, as compared to the more commonly used spherical NPs[13,14,18]. The sharp bands of SERS spectra obtained from selected Raman probes are ideal candidates for optical encoding, which can further facilitate multiplex and high-throughput immuno-detection[13,19].

Substrates commonly used in microfluidic devices and ELISA plates, such as polydimethylsiloxane (PDMS), polystyrene, or even glass, can lead to fluorescence or scattering background and partial overlap of vibrational bands from samples when using SERS tags for biological applications[20,21]. These traditional rigid substrates lack reusability and sensitivity, due to possible leaching of the randomly non-covalently attached antibodies. Flexible substrates such as paper for SERS can present several advantages over conventional rigid substrates, in terms of cost and processability, achieving Raman signal enhancements (EF ≈ 10^5–10^7) comparable with conventional supports[18,22]. Cellulose nanofibers are one of the most attractive green bioresources, due to their high abundancy, renewability, biodegradability, biocompatibility, and hydrophilicity. In particular, cellulose-based hydrogels are an attractive choice, not only due to low energy requirements for fabrication, but also by providing a smooth surface, highly appropriate for immunoassays due to the high water-absorption capacity[23]. Their moldability allows construction of microfluidic devices using simple fabrication methods, such as matrix-assisted 3D printing[24]. Importantly, cellulose-based hydrogels are transparent and have low background fluorescence, two essential characteristics for their application on highly-sensitive SERS-based microfluidics devices[25].

Finally, a POCT platform requires a simple readout of SERS spectra. A method that integrates data processing, analysis and readout should be applied to improve the limit of detection (LOD) and efficiency of SERS detection, even in the presence of high background signals. Although the conventional peak integral method still prevails in Raman data processing, multivariate curve resolution (MCR) methods are becoming increasingly popular[26–28]. These methods allow identification of the chemically meaningful components by demultiplexing the complete profile of Raman spectrum, improving the limit of detection and assay robustness[26,29]. The success of these methods has been demonstrated in digital SERS imaging for multiplex detection at ultralow concentrations[27].

In this work, we present a highly sensitive and selective SERS immunoassay using Horseradish Peroxidase (HRP) detection as a proof-of-concept analyte in a sandwich format. The strength of the reported SERS-based biosensor lies in merging:

i. SERS-immunotags based on gold nanostars, that proved to be strong SERS enhancers of the attached mercaptobenzoic acid (MBA) or 5,5′-dithio-bis(2-nitro-benzoic acid (DTNB) Raman probes. A highly active antibody corona was created by improving the method of covalent binding of antibodies to the Raman probe, giving rise to robust and stable SERS-immunotags.
ii. An easy to prepare, transparent, regenerated cellulose-based hydrogel (RCH) platform, to which capture antibodies were also bound by the same simple covalent approach as used on SERS-immunotags, generating a highly active capture platform.
iii. For SERS data analysis, we demonstrate the robustness of the simple Classical Least Squares method (CLS), in situations of partially overlapping key Raman bands derived from SERS-immunotags and the RCH platform. This approach allows quantitative mapping of the SERS signals along the capture platform and exclusion of interfering background signals.

Simultaneous detection of two unrelated antigens (duplexing) was also demonstrated, and shelf-live and reusability studies were conducted, in view of POCT microfluidics applications.

Results and Discussion

Design of the sandwich SERS-based immunoassay.

As illustrated in Figure 1A, the sandwich SERS immunoassay has two main components: (I) SERS-immunotags and (II) a capture platform. The preparation of the SERS-immunotags (Figure 1A, I) was performed in three steps, as previously reported[14], with minor changes: (1) synthesis of AuNSs[30]; (2) functionalisation of AuNSs with one of the two Raman reporters (MBA or DTNB) used for SERS detection, and (3) functionalisation with anti-HRP by covalent cross-linking mediated by 1-ethyl-3-(3-(dimethylamino)propyl)carbodiimide (EDC) and N-hydroxysulfosuccinimide (SNHS)[16,31]. To increase the specificity of HRP binding to SERS-immunotags, a blocking step with bovine serum albumin (BSA) was also performed[16].

The capture platform, based on regenerated RCH, was fabricated as previously described, with minor modifications[32]. After activation of the RCH membrane by partial oxidation/carboxylation of hydroxyl surface groups, immobilisation of anti-HRP antibodies was also performed by covalent crosslinking using EDC and SNHS[23](Figure 1Figure A, II). In order to increase the specificity of HRP binding to this capture platform, a blocking step with skim milk was performed[33].

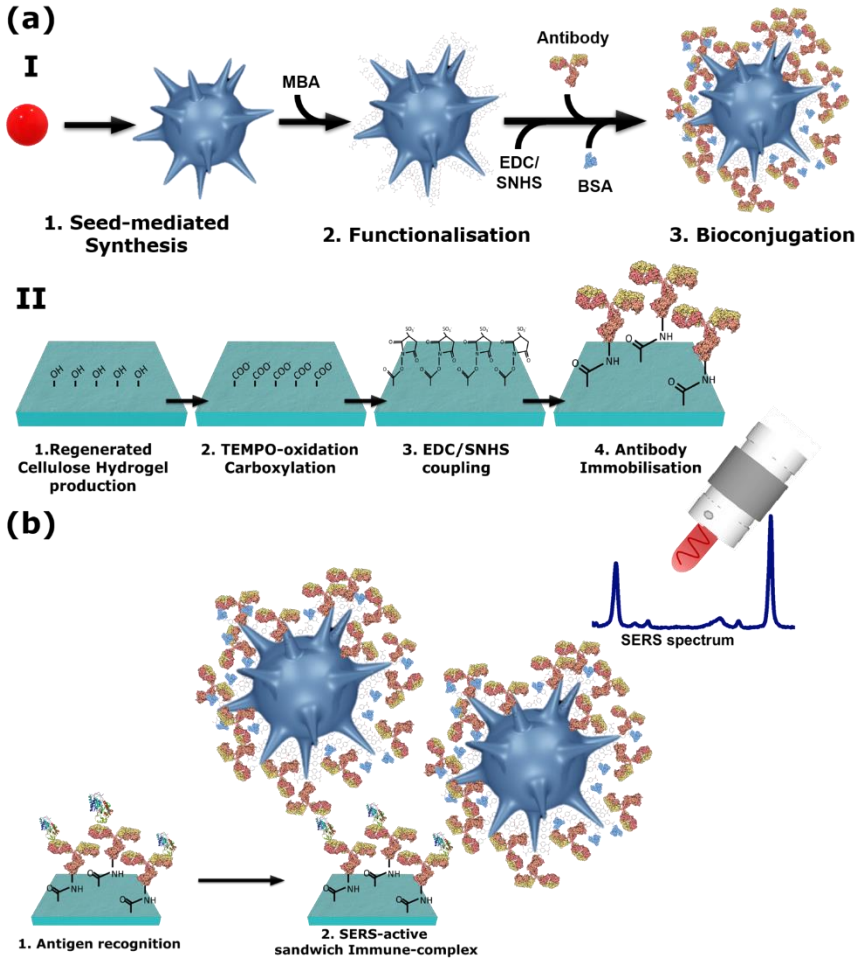

Figure 1 - Design of the sandwich SERS-based immunoassay. (a) Components of the immunoassay (I) Preparation of the AuNS-based SERS-immunotags; and (II) Fabrication of the capture platform, a TEMPO oxidised regenerated cellulose-based hydrogel (TO-RCH) membrane with immobilised antibodies. In both cases, functionalisation with anti-HRP antibodies was by cross-linking, mediated by EDC/SNHS. (b) Antigen recognition by the immobilised capture antibody and by the SERS-immunotags gives rise to a sandwich immunoassay complex. Quantification of antigen in the sample is made by detecting the SERS signal of immobilised SERS-immunotags.

Figure 1B is a schematic representation of the sandwich assay reported here. The sample containing HRP (antigen) is incubated with the capture platform, to allow for binding of HRP to immobilised anti-HRP antibodies. After washing, a solution containing SERS-immunotags is added, promoting the formation of the detection sandwich. After washing excess SERS-immunotags, quantification of HRP in the sample is performed by detecting the SERS signal of SERS-immunotags that remained immobilised in the platform.

Characterisation of the immuno-sensor components.

SERS immunotags. Gold nanostars (AuNSs) with an average tip-to-tip length of ≈ 70 nm were synthesised and characterised as previously reported[30]. These star-shaped gold nanoparticles were chosen based on the previous study, in which they showed excellent enhancement of Raman signal and batch-to-batch reproducibility[14]. AuNSs were characterised by UV-Vis, SEM and DLS (see Supplementary Information (SI), section 1). Functionalisation with each of the Raman reporters (MBA or DTNB) was performed as previously reported[14], and assessed by UV-vis spectroscopy and agarose gel electrophoresis (AGE) (see SI, section 2).

Functionalisation with the antibody, in this case anti-HRP, is a critical step to obtain highly efficient SERS-immunotags. Depending on the method used, the antibody molecules can bind to the surface of the nanoparticles in a random or oriented conformation, and this interferes with the ability to recognise and specifically bind the antigen. To obtain a highly efficient binding to HRP, the bioconjugation between SERS-probe-AuNSs and anti-HRP was performed using the EDC/SNHS method[31], and optimised by changing concentration of reagents, molar ratios between anti-HRP and AuNSs, reaction time and pH (see SI, section 3). A BSA blocking step finalised the SERS-immunotags preparation, ensuring minimal non-specific interactions[14].

The functionality of SERS-immunotags in the biosensor was assessed by measuring the enzymatic peroxidase activity of HRP bound to SERS-immunotags. Four different concentrations of anti-HRP antibody were used to prepare SERS-immunotags, corresponding to 53, 105, 211 and 422 nM for 0.2 nM AuNSs. Incubation of these SERS-immunotags with an equimolar amount of HRP (based in the amount of anti-HRP), was followed by a washing step by centrifugation/resuspension, and HRP

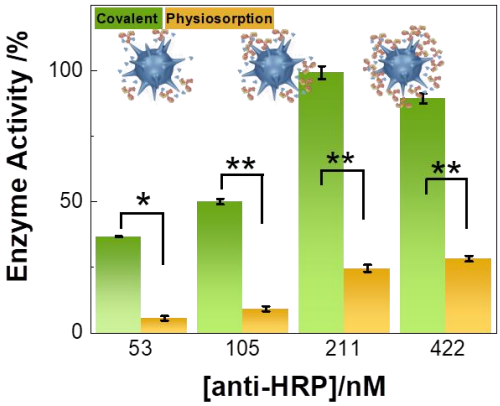

Figure 2 - Functionality of the SERS-immunotags obtained by physiosorption (yellow bars) or covalent (green bars) methods, as evaluated by percent enzyme activity of bound HRP relative to free HRP. Four concentrations of anti-HRP, 53, 105, 211 and 422 nM, bound to 0.2 nM AuNSs, were incubated with HRP, followed by washing. Controls without HRP showed no enzymatic activity. For the maximal relative enzymatic activity (SERS-immunotags with 211 nM anti-HRP), covalent conjugates are *ca.* 5 times more active than their physiosorbed counterparts. One-way analysis of variance (ANOVA) was applied for statistical comparison followed by the Tukey's multiple comparison test, *$p \leq 0.05$, **$p \leq 0.01$.

enzymatic activity was measured[14]. Figure 2 shows the relative enzymatic activity of the HRP-bound to SERS-immunotags, for all anti-HRP concentrations used, in comparison to HRP-bound to SERS-immunotags prepared with the same concentrations, but by a physisorption method[14]. For both types of SERS immunotags, maximal relative enzymatic activity was reached for 211 nM anti-HRP, not changing appreciably for the higher anti-HRP concentration tested (422 nM). A concentration of 211 nM anti-HRP was thus considered to be appropriate to prepare highly active SERS-immunotags. Covalent conjugation was favoured, as those SERS-immunotags were ca. five times more active than their physisorption counterparts (Figure 2). Interestingly, this increase in enzymatic activity obtained for our covalent SERS-immunotags relative to their physiosorbed counterparts, is similar to that obtained for conjugates of protein-A mediated anti-HRP antibody immobilisation on 60 nm spherical gold NPs[17]. The use of protein-A allows orientation of antibodies at the surface of the NPs in a favourable position for antigen binding. Possibly, the reason for a favourable orientation of anti-HRP antibodies, in our case, is the low pH used for the EDC/SNHS coupling reaction. In fact, using a pH lower than the pI value induces rapid electrostatic adsorption in the correct orientation of the antibody molecules to the negatively charged surface of the AuNSs[16].

To further assess the activity of the sandwich formation between SERS-immunotags, HRP and anti-HRP, the electrophoretic mobility of AuNSs, SERS-immunotags, SERS-immunotags with bound HRP and further bound to anti-HRP (a solution simulation of a positive sandwich assay) were measured by AGE[14,15,34,35]. Results on SI, Figure S7, are a proof-of-principle for application of the SERS-immunotags to the SERS-based immunoassay.

Capture platform. RCH membranes were prepared by previously published methods, with minor modifications[32], by shear-casting dissolved cellulose on a cleaned glass plate, followed by treatment with glacial acetic acid. The robust membrane thus obtained is transparent, a desirable feature for integration into microfluidics devices[36] (see inset in Figure 3A). As opposed to other cellulose-based substrates, no interfering fluorescence from additives of paper manufacturing production is present, a major advantage for sensitive Raman measurements[18]. The RCH membrane thickness was ≈ 43.5 µm, as evaluated by SEM (Figure 3B). Before immobilisation of anti-HRP, the membrane was activated by oxidation of the hydroxyl surface groups to carboxylic moieties, using the 2,2,6,6,-tetramethylpipelidine-1-oxyl radical (TEMPO)/NaBr/NaClO in water at pH 10–11[37]. This is an efficient and selective conversion reaction, that can be used in large scale processes providing the required surface carboxylic groups for EDC/SNHS cross-linking[23].

Scanning Electron Microscopy (SEM) micrographs in Figure 3A and 3B, show the topography of the hydrogel membrane, with a reasonably smooth surface formed by several stacked layers of regenerated cellulose. Comparing unmodified RCH with the activated, TEMPO-oxidised RCH (TO-RCH), the cellulose structure seems to be covered by a "gel-like" layer after activation, leading to an increase in surface roughness from 67.3 nm for the unmodified-RCH to 84.3 nm for TO-RCH, as evaluated by AFM (Figure 3C and 3D, and SI, section 5). The RCH membrane was also characterised by FTIR (SI, Figure S8) before and after oxidation. Results show the typical vibrational bands from cellulose, with the appearance of carboxyl bands in the 1600-1700 cm^{-1} region after oxidation[38].

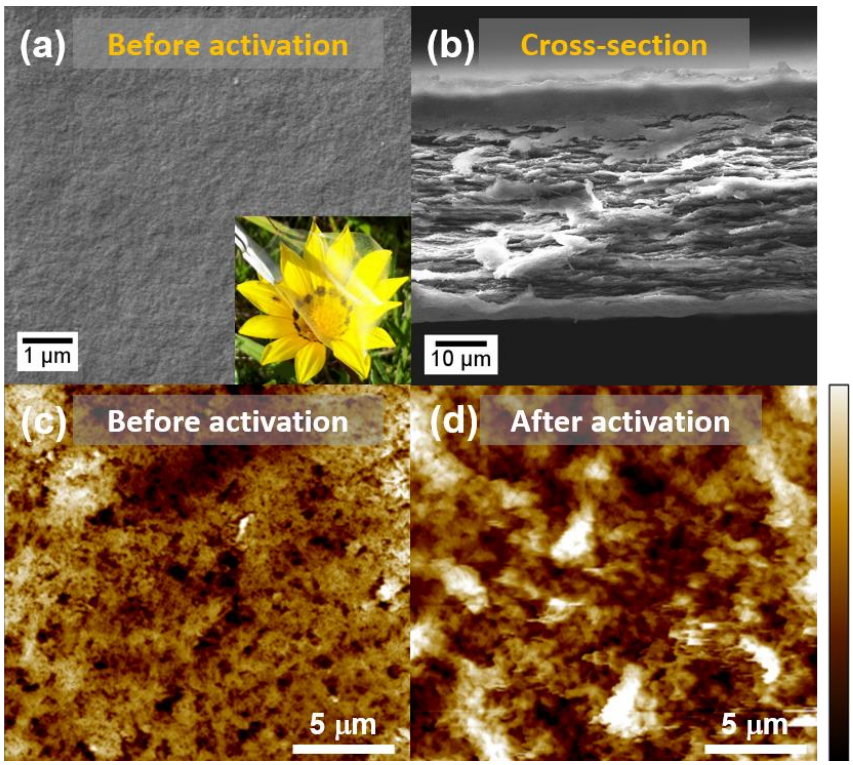

Figure 3 - SEM micrographs from the (a) surface and (b) cross-section of the as-prepared RCH. The inset in (a) is a photograph of the as-prepared RCH in front of a flower, evidencing its transparency. AFM topography images of surfaces from RCH before and after oxidation for antibody immobilisation: (c) As-prepared RCH (maximum height of 400 nm); (d) Activated, RCH after treatment with TEMPO (TO-RCH) (maximum height of 1200 nm).

Functionalisation of the TO-RCH platform with antibodies was performed by both physisorption and a covalent method, with further blocking with skimmed milk to increase the specificity of antigen recognition by the immobilised antibodies. The efficiency of covalent anti-HRP immobilisation on the platform was evaluated upon capture of HRP, by measuring the enzymatic activity, and compared with immobilisation of anti-HRP by physisorption on an equivalent platform. As shown in Figure 4**Error! Reference source not found.**A, the enzymatic activity of the HRP on the capture platform obtained by covalent anti-HRP immobilisation (green bar) is *ca.* twice that observed for the corresponding platform obtained by physisorption (yellow bar). This difference can be explained by a combination of two effects, namely, i) the covalent-binding approach allows for a correct orientation of the anti-HRP antibodies, maximising HRP binding; and ii) physiosorbed antibodies can be bleached during the washing procedure following their immobilisation[39]. As a blocking control, the enzymatic activity of the HRP on the platform without anti-HRP (TO-RCH alone, grey bar), was found to be residual, confirming efficient blocking of the platform.

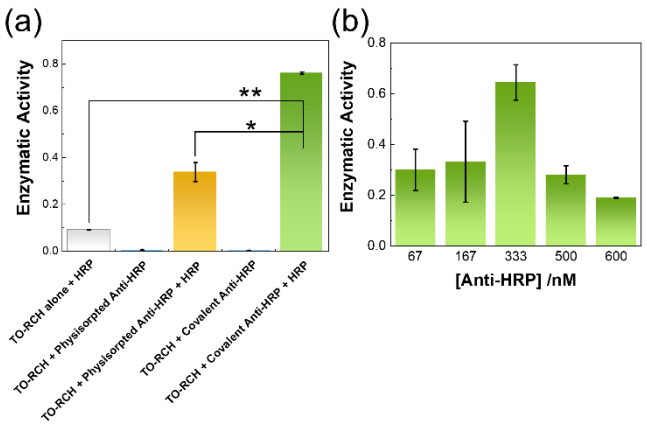

Figure 4 - HRP enzymatic activity evaluates anti-HRP antibodies immobilisation on TO-RCH. (a) Covalently-bound antibodies (green bar) have double the HRP activity that their physiosorbed counterparts (yellow bar). The residual activity from HRP bound to TO-RCH alone (grey bar), and the lack of activity in samples without HRP confirms efficient blocking of the platform, and that HRP is in fact bound to anti-HRP antibodies in the two other cases. (b) Different anti-HRP concentrations allow optimisation of HRP capture efficiency. Error bars correspond to the standard deviation from three independent experiments (different sets of SERS-immunotags). One-way analysis of variance (ANOVA) followed by the Tukey's multiple comparison test were applied for statistical comparisons. ∗p≤0.05, ** p≤0.001.

Moreover, this residual activity from HRP adventitiously bound to the TO-RCH platform, confirms that HRP is in fact bound to anti-HRP antibodies in the two other cases in which antibodies are present.

To optimise the capture of HRP to the platforms, the concentration of anti-HRP used in the chemical cross-linking procedure was varied from 10 to 90 $\mu g.\mu L^{-1}$ (Figure 4B). Upon HRP binding, maximum enzymatic activity was found for an antibody concentration of 50 $\mu g.\mu L^{-1}$. The decrease in enzymatic activity for higher concentrations indicates that steric hindrance of the antibodies compromises the binding of the antigen. This is a factor which must be taken into consideration in defining the limit of detection of the present biosensor. In further experiments, we thus decided to use TO-RCH capture platforms with covalently bound anti-HRP antibodies, at a concentration of 50 $\mu g.\mu L^{-1}$.

SERS-based immunoassay.

Characterisation of the sandwich immuno-complex. To characterise the formation of the sandwich immuno-complex at the capture surface, Atomic Force Microscopy (AFM) images were obtained to compare the capture platform containing anti-HRP, and the platform containing the sandwich immunocomplexes formed in the presence HRP and SERS-immunotags (Figure 5A and 5B). The capture platform shows globular features homogeneously distributed over the surface, with diameters around 40 nm, which are absent in the AFM images of TO-RCH before antibody immobilisation (Figure 3D). These features are bigger than expected, based on the diameter of the free antibody in solution (≈16 nm), which may be explained by the convolution effect of the AFM probe (tip≈14 nm), and also by the roughness of the bare TO-RCH surface, that precludes a rigorous measurement of the size of small features.[23,40] When HRP and SERS-immunotags are added to form the sandwich immunocomplex, the diameter of these globular features increases to ≈150 nm (Figure 5B), a size within the expectable range for the sandwich immunocomplex. Further corroboration of the presence of sandwich immunocomplexes was obtained by SEM coupled with Electron Diffraction Spectroscopy (EDS), by the detection of gold at the globular aggregates, confirming the presence of AuNSs from the SERS-immunotags and thus the identity of these aggregates as sandwich immunocomplexes (Figure 5C and 5D).

The sandwich immuno-complexes were also characterised by Raman spectroscopy, to evaluate the feasibility of the present sensor. Figure 6 shows Raman spectra of the as-prepared TO-RCH platform, and of the platform after covalent immobilisation of anti-HRP. For comparison, SERS spectra of the SERS-immunotags (with MBA as Raman reporter) deposited onto a glass surface and of the total sandwich immunoassay, are also presented. SERS spectra of MBA in the SERS-immunotags and in the sandwich immunoassay, show two highly enhanced sharp bands at 1079 and 1590 cm^{-1}. In this spectral region, the capture platform shows a strong Raman band at 1097 cm^{-1}, with weaker shoulders up to 1160 cm^{-1} and weaker broad bands in the 1200-1500 cm^{-1} region (Figure 6). Raman spectra of the TO-RCH platform have a much lower intensity that the SERS signal from the MBA reporter in the SERS-immunotags, as is

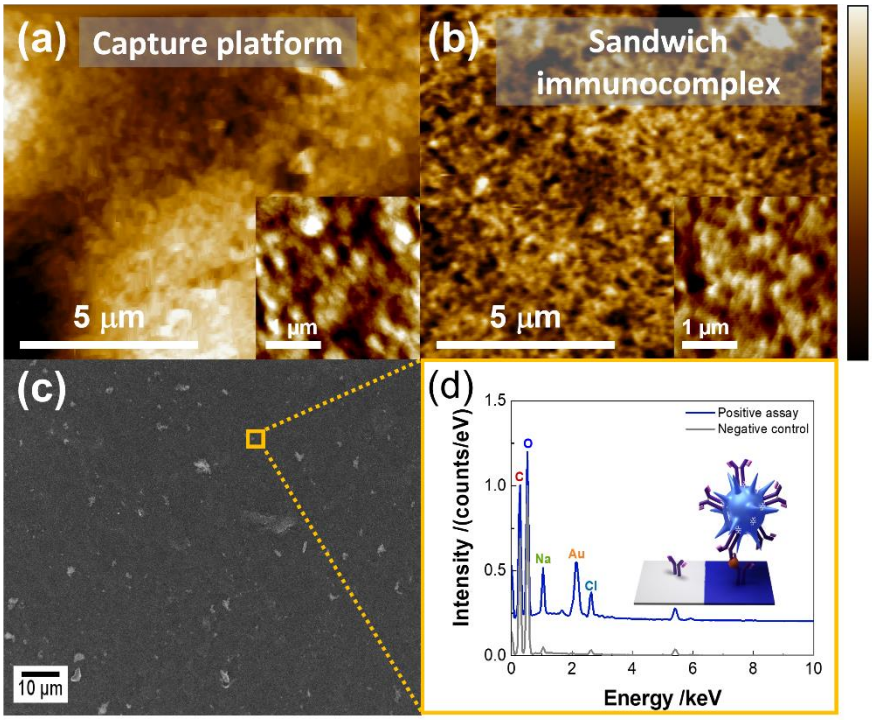

Figure 5 - AFM topography images of surfaces from (a) Capture platform i.e. TO-RCH platform functionalised with anti-HRP (maximum height of 500 nm, inset maximum height of 60 nm); (b) Sandwich immunocomplex, i.e., capture platform as incubated with the antigen, HRP, and then incubated with the SERS-immunotags to form the sandwich immunocomplex (maximum height of 300 nm, inset maximum height of 60 nm). (c) SEM image of the surface with a positive sandwich immunocomplex assay; (d) Comparison between EDS spectra of sandwich immunocomplex assay (blue trace) and the negative control (grey trace). The blue spectrum was taken from the area highlighted by a yellow square in (c).

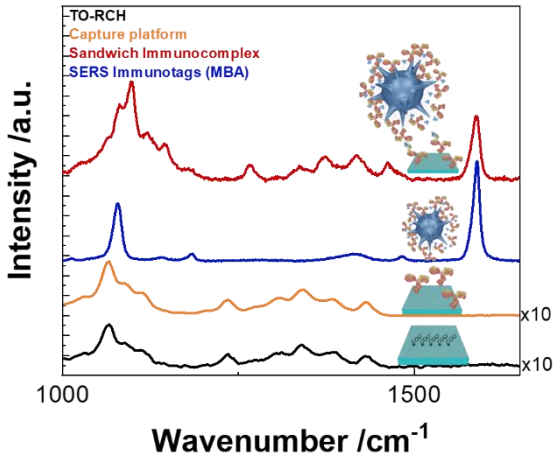

Figure 6 - Relevant Raman and SERS spectra. From bottom to top: 10 x amplified Raman spectra of the as-prepared TO-RCH platform (black) and of the capture platform, i.e., after covalent immobilisation of anti-HRP (orange); SERS spectra of SERS-immunotags with MBA as Raman reporter (blue), and of the total sandwich immunoassay (red).

noticeable in Figure 6, in which these spectra are represented with a 10-fold signal amplification. Nevertheless, platform contribution to the background signal, the strongest band at 1097 cm^{-1}, can partially overlap with the 1079 cm^{-1} band of MBA, and can be falsely attributed to the MBA signal, leading to a decrease in biosensor performance.

Interference from the background and low reproducibility are two of the major drawbacks for the successful implementation of SERS as a highly sensitive detection technique[20]. To overcome these issues, we used a combination of two approaches. First, SERS data were collected using a point mapping method, in a scan of 21 x 21 mm, in triplicate, with a total of 1233 pixels per sample. This approach allows the detection of a larger number of reporter signals, reducing the problem associated with inhomogeneity of the sample, and avoiding prolonged laser illumination that may lead to photodecomposition. The second strategy was to use the CLS (see SI, section 6 for details), for efficient removal of the background signal arising from the platform. CLS has been reported as a suitable method to resolve complex spectra even in high background situations[28], allowing for accurate quantification of the SERS signals from the SERS-immunotag, even at very low concentrations. The method relies on spectral deconvolution, using as references, both the Raman spectrum of the capture platform and the SERS spectrum of the SERS-immunotag.

Figure 7**Error! Reference source not found.**A shows SERS spectra of the capture platform after incubation with HRP and SERS-immunotags, *i.e.*, the total sandwich immunoassay. HRP concentration was varied between 0.01-0.10 $ng{\cdot}mL^{-1}$, and SERS maps were performed in three different areas for each sample. Figure 7B shows a comparison between the CLS method *vs.* peak integral method using either the 1079 or the 1590 cm^{-1} bands, for SERS data analysis. Both methods provide a linear correlation between the intensity of the probe and the concentration of HRP, but for the CLS method the coefficient of determination (r^2) is 99.6% *vs.* 87.4% or 88.3% for the band integral method using the 1079 or the 1590 cm^{-1} bands, respectively. When applying the CLS method, a threshold value of 0.352 component coefficient was established for positive detection (see SI section 7). This was important to minimise the error for the components tested, as well as loss of information from the dataset[41].

The advantage of using the CLS method for low concentrations of HRP is evident in Figure 7C, in which the deconvolution of the experimental spectrum using CLS is compared with experimental data. As can be clearly seen, CLS can demultiplex and allow quantification of the signal from SERS-immunotags at low concentrations, decreasing the influence of overlapped bands from the background. The fitting result indicates that the CLS best-fit spectrum can reproduce all bands both from the SERS-immunotags and the platform, that are present in the experimental spectrum.

Figure 7D shows two pixelated SERS maps obtained in the presence or absence of HRP. The higher the CLS score, the more intense is the blue colour, indicating that HRP has been specifically detected. The low counts in the control sample show that non-specific binding of the SERS-immunotags to the platform is negligible, confirming that the assay is highly specific to detect and quantify HRP.

The limit of detection (LOD) and the limit of quantification (LOQ) of the immunoassay, were calculated by the standard IUPAC method as 7.5 ± 0.5 $pg{\cdot}mL^{-1}$ and 33.2 ± 0.2 $pg{\cdot}mL^{-1}$, respectively[42]. The major sensing properties of this work were compared with other detection systems and have been summarized in Table 1. These results further confirm the robustness of our immunoassay, making our biosensor superior to enzyme-linked immunosorbent assay (ELISA), and other SERS immunoassays[4,43] and comparable to others[44]. Our RCH-based platform is also more sensitive, stable, and easier to fabricate and regenerate, than alternative designs[2,3,7,45,46].

Table 1 - Comparison of the sensitivity of analytical methods for SERS-based immunoassay detection.

Analytical method	Limit of detection (LOD)	References
Enzyme-Linked Immunosorbent Assay (ELISA)	2 mg·ml^{-1}	47
Magnetic SERS immunoassay	10.0 ng·ml^{-1}	4
Vertical flow paper-based SERS immunoassay	3 ng·ml^{-1}	43
Hydrophobic paper-based SERS immunoassay	9 pg·ml^{-1}	44
Molecularly imprinted polymer (MIP) based sensors	100 pg·ml^{-1}	45
Electrochemical biosensors	2.7 μg·ml^{-1}	46
Paper-based microfluidics systems	47 pg·μL^{-1}	7
SERS-improved Lateral Flow Assay	0.073 ppb	2
Paper-based SERS assay	0.1 pg·ml^{-1}	3
TO-RCH capture platform	7.5 ± 0.5 pg·ml^{-1}	This work

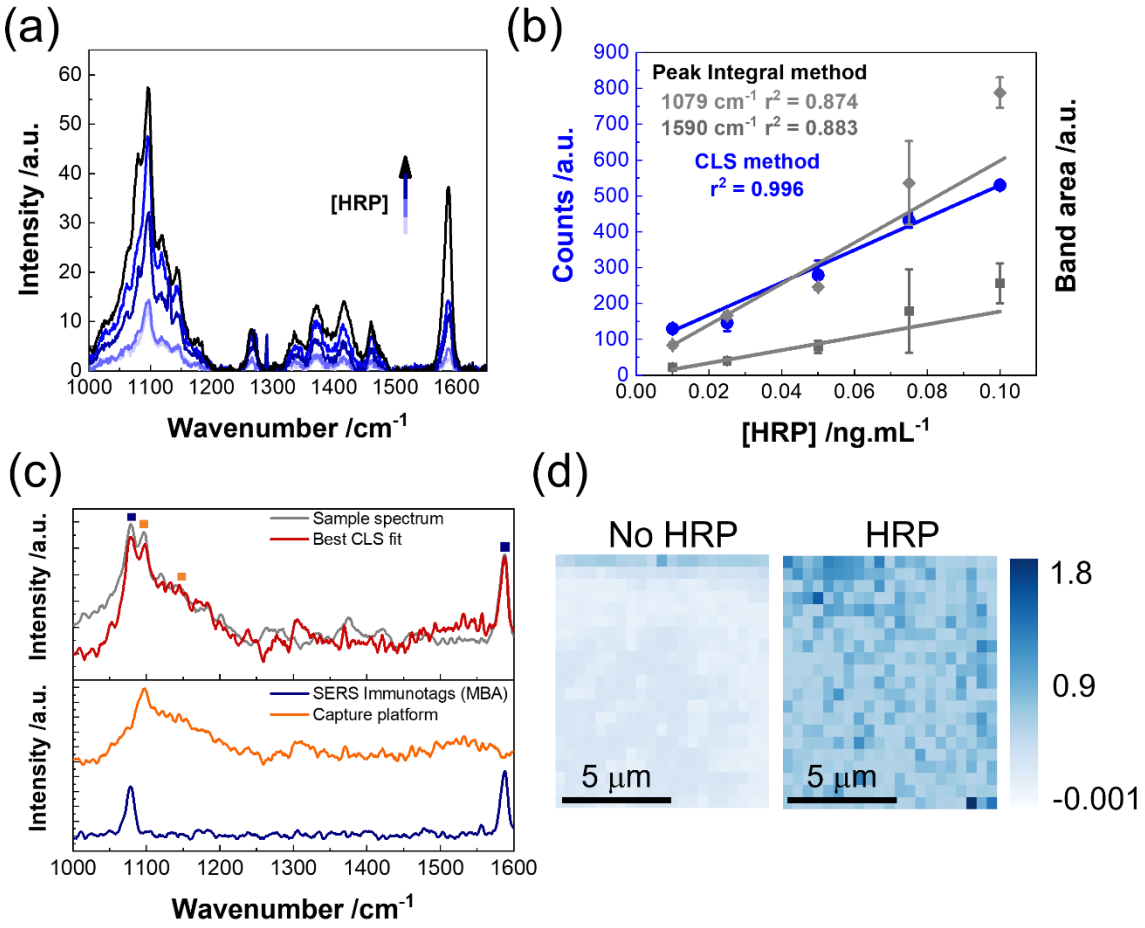

Figure 7 - Data treatment of SERS results for the sandwich immunoassay applied for HRP concentrations in the range 0.01-0.10 ng·mL^{-1} (a) Average SERS spectra for each HRP concentration; (b) Linear fit and corresponding SERS counts from the immunoassay, obtained by the CLS method (blue points and line with a coefficient of determination r^2 = 99.6%), or by the band integral method (grey points and lines with a coefficient of determination r^2 = 87.4% for the 1079 cm-1 band; and r^2 = 88.3% for the 1590 cm^{-1} band). Error bars indicate the standard deviation of three independent experiments. (c) Top: Measured multiplexed SERS spectrum (grey) and the best-fit spectrum by the CLS algorithm (red). Blue squares indicate SERS bands from MBA signal of the SERS-immunotags and orange squares bands indicate Raman from the capture platform. Bottom: Demultiplexed pure Raman spectra of MBA and the capture platform, from the best-fit spectrum. (d) pixelated SERS maps obtained in the presence or absence of HRP. The higher the CLS score, the more intense is the blue colour.

Reproducibility and selectivity of the immunoassay. The inter and intra-reproducibility of the SERS-based immunoassay were evaluated by performing the immunoassay using three independent batches of TO-RCH platforms. Similar responses were obtained between different batches and within each batch with a relative standard deviation for the SERS signal of 13%, indicating a high reproducibility between the four performed immunoassays for each sample (Figure S11).

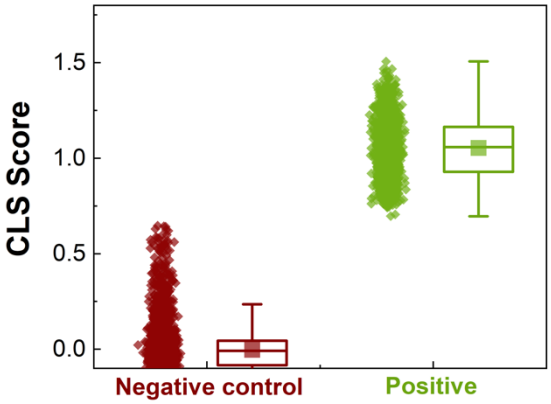

Figure 8 - Selectivity response of the immunoassay based on classical least squares (CLS) results. The CLS technique was used to quantify the contributions of a "Negative control" (red data), obtained when using an irrelevant antigen (PfHRP2) and a "Positive" (green data) for the target antigen, HRP. In the box plots, squares are the mean value for each distribution, the middle line represents the median and the top and bottom lines of each box represent the 75 and 25 percentile values, respectively. Whiskers show upper and lower adjacent values which is 3×IQR (Interquartile Range). Nonparametric analysis of variance by Kruskal-Wallis test (ANOVA) was performed for statistical comparisons. *p≤0.05.

The selectivity of the SERS-based RCH immunoassay was assessed by testing the responses to a purified irrelevant antigen, namely *P. falciparum* His-Rich Protein 2 (*Pf*HRP2), used for malaria infection detection[48] *vs.* positive detection using the target antigen, HRP (Figure 8 and Figure S12**Error! Reference source not found.**). The low coefficients (mean of 0.05) obtained show a negative response for the non-target antigen, whereas the high coefficients (mean of 1.05) represent the positive detection of the target antigen. As can be seen in Figure 8, high CLS scores SERS signals are only obtained in the presence of the immuno-complex, confirming an excellent and consistent selectivity response in detecting the presence of the intended antigen, HRP.

Duplexing detection. A duplexed SERS immunoassay was performed to further demonstrate the versatility and usefulness of the proposed system. Two SERS-immunotags containing, two different Raman reporter molecules (DTNB and MBA) and two different antibodies (anti-HRP and anti-*Pf*HRP2), respectively were incubated with a TO-RCH platform containing similar amounts of both antibodies covalently bound. Usually, the SERS signals from several reporters are identified and quantified by the peak integral method, which relies on separated specific bands[2,3,49]. In fact, the two Raman reporters present fairly separated specific Raman bands (*e.g.*, MBA: 1588 cm^{-1} and DTNB: 1335 cm^{-1}). However, they also have other bands with a partial overlap (between 1063 and 1079 cm^{-1}), which is around the broad band at 1098 cm^{-1} related to the weak cellulose spectra. By applying the CLS method, it was possible to resolve the mixed spectra from each pixel. CLS coefficients for MBA, DTNB and the RCH membrane from all the pixels were plotted in a coloured scheme in Figure 9**Error! Reference source not found.**. Also in this duplexing application, the CLS method was able to identify and clearly distinguish the two specific SERS reporters from the background, in contrast with the peak integral method, as illustrated for example by the work of Tan *et al.*[28].

Stability and reusability of the capture platform. The stability of the SERS-immunotags and of the capture platform are critical factors for the application of the biosensor. Therefore, the antigen-binding ability was monitored independently by measuring the enzymatic activity after HRP-binding for SERS-immunotags or the capture platform after 16 h, 24 h and 168 h (one week), after the respective preparation. The SERS activity of the sandwich immunoassay was also monitored at the same time points (Figure S12). The anti-HRP antibodies bound to the capture platform showed great stability, retaining 83% of their initial binding activity, even after one week of storage. This high stability might be attributed to intermolecular cross-linking as already reported by others[23]. The SERS-immunotags, after one week, showed 52% of their original binding activity, a drop probably due to some agglomeration occurring in their stock solution. In terms of the SERS activity of the sandwich immunoassay, it did not vary appreciably after 24 h, and it was reduced by only 13% after one week (Figure S12). These results underscore the excellent properties of the RCH platform, providing a high-water content environment that contributes to biomolecules stabilisation. This is an advantage over many polymer matrixes and other functional surfaces (*e.g.* ELISA plates, paper-based substrates and glass) used for immobilisation[23].

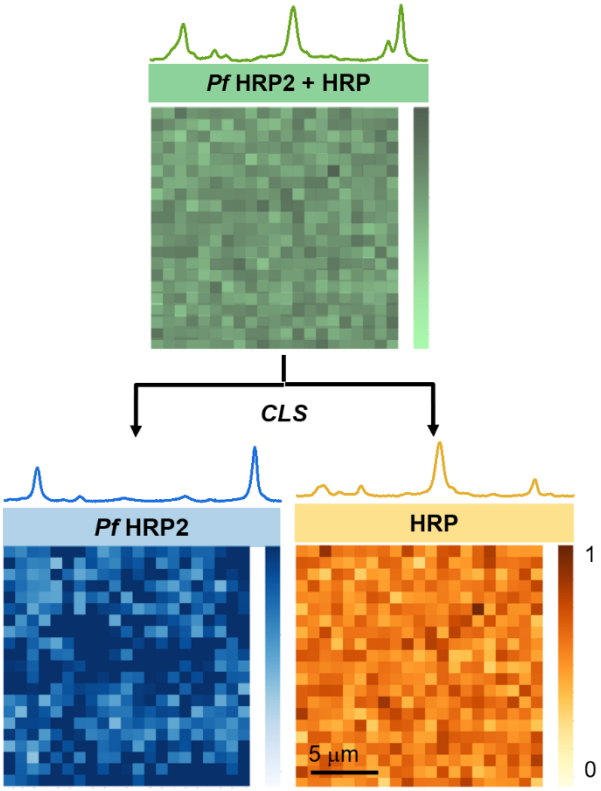

Figure 9 - Pixelated SERS maps for duplexing detection. Top: Green map of an immunoassay containing equimolar amounts of anti-PfHRP2 and anti-HRP antibodies in the capture platform, equimolar amounts of the respective antigens in the assay solution, and equimolar amounts of MBA-SERS-immunotags containing anti-PfHRP2 antibodies and DTNB-SERS-immunotags containing anti-HRP antibodies. Bottom: The CLS method allowed excellent data deconvolution of the green map into its blue (PfHRP2 detection) and yellow (HRP detection) components. Reference SERS spectra of the contents are represented above each pixelated SERS-map.

The ability to consecutively reuse the biosensor was also studied (see section 9, SI). Even after seven analytical cycles, the SERS activity of the sandwich immunoassay was 87% of the value obtained in the first assay of the cycle (Figure S13 and S14). Although no consensus exists on defining a successful regeneration process[50], our cellulose-based SERS immunoassay was able to retain its activity over several cycles while reducing the overall cost of the SERS immunoassay, a feature absent in other paper-based assays[3,51], thus proving to be suitable for repeated sensing applications in POCT, with minimal activity loss.

Conclusions

In this work, we present a highly sensitive and selective SERS immunoassay using HRP detection as a proof-of-concept analyte in a sandwich format. SERS-immunotags were based on AuNSs, a type of plasmonic NPs that associate the stability of gold with the exceptional Raman-enhancing properties of its hot-spots. These AuNSs were functionalised with the Raman probes MBA or DTNB, well known for their high Raman cross-sections. Our approach for covalent attachment of antibodies, guaranteed a 5-fold increase in their biological activity in the final SERS-immunotags (as compared to attachment of antibodies by physiosorbion[14]), without the need for more expensive and laborious procedures, such as protein-A based immobilisation. Moreover, the approach to perform these functionalisation reactions in solution, leads to high reproducibility of the SERS signal and hints at easier scalability, compared to conventional methods of surface chemistry. The capture platform was easily prepared from regenerated cellulose-based hydrogel platform, a renewable and transparent material with low background fluorescence. Capture antibodies were also bound by the same simple covalent approach as used on SERS-immunotags, and here presented double biological activity as compared to physiosorbed antibodies. The presence of the sandwich complexes on the platform during a detection event, was confirmed by the detection of globular features by AFM. SEM/EDS, allowed to associate these globular features with the presence of gold, further confirming their identity. For SERS data analysis, we demonstrate the robustness of the CLS method, in situations of partially overlapping key Raman bands derived from SERS-immunotags and the RCH capture platform. In fact, application of the CLS method to SERS data treatment revealed superior discrimination of Raman probes signals from the background, a serious disadvantage of the more commonly used peak integral method. Also, CLS allowed a much better data fit in antigen concentrations in the 0.01 to 0.1 ng.mL^{-1} range. The CLS method was also advantageously applied to a duplexing application of our SERS-immunosensor, as compared to peak integral method, and opens the way for multiplexing applications. Our developed SERS-based immunoassay greatly improves the detection limits of traditional ELISA approaches,

from mg to pg levels of detection, and its performance is better or comparable to other SERS-based immunosensors reported in the literature. The reusability of the capture platform reduces implementation cost of the biosensor, thus increasing its commercial attractiveness, while it also represents an environmentally sustainable option. The capture platform can withstand at least 7 cycles of regeneration, making it highly attractive for future POCT microfluidics applications.

In conclusion, our approach at SERS immunoassay construction could successfully overcome the main challenges for application at POCT, including increasing reproducibility, sensitivity, and specificity, associated with an environmentally friendly and robust design. Also, the proposed design opens the way for multiplexing applications on a microfluidics POCT platform.

Experimental

Materials.

The following reagents were used: Gold(III) chloride solution 30% wt. Au in dilute hydrochloric acid (99.99%), sodium citrate tribasic dihydrate (99.0%), silver nitrate (99.9999%), Tris(hydroxymethyl)-aminomethane, ethylenediaminetetraacetic acid, acetic acid (≥ 99%), ethanol, the Raman reporters of 4-mercaptobenzoic acid and 5,5-dithio-bis-(2-nitrobenzoic acid), the crosslinking reagents, buffers (2-(n-morpholino)ethanesulfonic acid, phosphate-buffered saline and potassium phosphate buffer), as well as the reagents used in RCH preparation and in antibody immobilisation protocol (namely, lithium hydroxide (≤98%), microcrystalline cellulose (powder: 20 μm), 2,2,6,6,-tetramethylpipelidine-1-oxyl radical, sodium bromide, sodium hypochlorite, bovine serum albumin, skim milk powder, Tween 20, poly-l-lysine solution, horseradish peroxidase (HRP) were all purchased from Sigma-Aldrich, St. Louis, USA. The anti-HRP antibody was from Antibodies-Online, Germany. Urea (≥ 99.5%) was purchased from Carl Roth GmbH, Germany. Enzymatic assay reagents, 2,2'-azino-bis(3-ethylbenzothiazoline-6-sulfonic acid) was from Roche, France and hydrogen peroxide (30%) and nitric acid (65%) by Panreac AppliChem, Germany. L-ascorbic acid (99.9%) was purchased to Fluka, Buchs, Switzerland. Protein determination was by the bicinchoninic acid method (based on Smith *et al.*[52]) using a kit from Sigma-Aldrich, St. Louis, USA. Ultrapure™ Agarose was from Invitrogen—Thermo Fisher Scientific, Waltham, USA. All chemicals and reagents were of the highest purity available. Ultrapure water (18.2 MΩ·cm at 25 °C) was used for the preparation of all solutions, unless stated otherwise.

Preparation of gold nanostars and SERS-immunotags.

Gold nanoparticles synthesis and functionalisation. The synthesis of gold spheres and star-shaped nanoparticles were performed according with the proposed methods of Ojea-Jiménez *et al.*[53] and Yuan *et al.*[30], respectively. The functionalisation was performed as described in Oliveira *et al.*[14]. Detailed information can be found in section 1 of SI.

SERS-immunotags with covalently attached antibodies. To promote crosslinking of the carboxylic acid groups of MBA or DTNB (MBA/DTNB) to the primary amines from the anti-HRP antibody molecules, several parameters were optimised, namely pH, reaction time, concentration and molar ratios of the reagents. The typical procedure to produce AuNS–MBA/DTNB–anti-HRP SERS-immunotags was executed as follows: AuNS-MBA/DTNB – 0.2 nM - were washed by centrifugation at 2500 g at 4 °C for 10 min and resuspended in 5 mM MES buffer pH 6.5. A volume of 10 μL and 20 μL of EDC and SNHS at 1 mM was added to the colloidal suspension and let to react for 15 min in an orbital shaker (Biosan TS-100, Latvia) at 700 rpm at 25 °C. Following the carboxylic group activation, anti-HRP was added in appropriate amounts of antibody to obtain SERS-immunotags with a [AuNSs]:[anti-HRP] molar ratio of 1:422[14]. The spent carbodiimide from AuNS–MBA/DTNB–anti-HRP, is removed through centrifugation. The incubation was also performed in an orbital shaker at 250 rpm, at 25 °C. Samples were then centrifuged for 10 min at 4 °C and 2500 g. The supernatant was discarded to remove excess protein and resuspended in 5 mM phosphate buffer pH 7.4. The blocking step was achieved through BSA to block non-specific interactions at the same molar ratio used for the anti-HRP. The AuNS–MBA/DTNB–anti-HRP–BSA conjugates, are referred as "SERS-immunotags". These SERS-immunotags were then used to incubate with HRP and/or anti-HRP to simulate the sandwich immunoassay. Incubation and wash steps were performed as done to form the SERS-immunotags.

Regenerated Cellulose Hydrogel for antibody immobilisation. Based on procedures reported in the literature for the dissolution of cellulose[32,54,55], the cellulose dissolution medium was prepared by mixing 4.6 wt.% LiOH, 15 wt%. urea in 80.4 wt.% deionised water. The solvent mixture was pre-cooled in a freezer at -25 °C, until it becomes a frozen solid. The frozen solution was then allowed to thaw at RT, and 6 wt.% of microcrystalline cellulose (MCC) (powder: 20 μm) was immediately added into the solvent system under vigorous stirring at -8 °C until its complete dissolution (≈ 30 min). A freezing-thawing cycle was performed to improve cellulose dissolution. Then, 5 mL of the resulting viscous solution was evenly spread on a glass plate (10×10 cm^2), and cellulose was regenerated for 60 min with glacial acetic acid. The sheet-like hydrogel membrane was thoroughly washed with deionised water to remove the remaining salts, dried at room temperature for 3 days and stored in air.

In order to immobilise antibodies, the RCHs were oxidised by using TEMPO/NaBr/NaClO system as described by Isogai *et al.*[37]. Firstly, 52 mL of ultrapure water were added to approximately 1 g of RCH. TEMPO and NaBr were dissolved and added to a final concentration of 2.5 mM and 15.28 mM, respectively. Then, 879.68 mM of NaClO were added in the solution and the pH was adjusted to 10 by adding 0.5 M NaOH. The TEMPO-oxidised RCHs (referred as "TO-RCH") were kept in the solution for 1 h under vigorous stirring (≈700 rpm). Finally, the TO-RCHs were thoroughly washed in ultrapure water and kept at room temperature in a solution of 10% of H_2O_2.

The TO-RCH was made amine-reactive via EDC/SNHS activation to couple antibodies as follows: the hydrogel was washed with ultrapure water and immersed in 100 μL of 10 mM MES buffer pH 6.5. EDC/SNHS activation was achieved through the protocol

described by Dixit *et al.*[56]. Volumes of 100 μL of EDC and SNHS at 20.86 mM and 50.66 mM, respectively, were allowed to react with the hydrogel for 15 min in an orbital shaker at 250 rpm, at 25 °C, and the volume was discarded. Afterwards, 100 μL of antibody at 50 $\mu g.mL^{-1}$ in MES buffer 10 mM pH 6.5 were added. The solution was mixed with the pipette and incubated for 15 min in the orbital shaker. The sample was left incubating overnight at 4 °C. The crosslinking reaction was stopped by washing three times the TO-RCH with 20 mM PBS buffer at pH 7.4 to remove electrostatically bound antibodies. A volume of 100 μL of skim milk as blocking agent at 0.5% (w/v) with Tween 20 at 0.05% (w/v) was added to the membrane and incubated in the orbital shaker for 30 min at 25 °C. Since the antibody used herein is polyclonal *i.e.* is able to recognise multiple epitopes, the ratio between antibody and antigen can be considered as 1:1[16]. Therefore, 100 μL of 50 $\mu g.mL^{-1}$ of HRP were incubated for 30 min at 25 °C and then the hydrogel was washed as previously described for the crosslinking reaction. Special attention was taken during the washing steps, as it is essential in ELISA assays to remove unbound material[9]. Washing was done with buffer three times, after which the washing solution was removed completely. Antibody concentration was optimised to maximise the response of the substrate. The SERS-based sandwich immunoassay was finalised by incubation of 1 nM of SERS-immunotags for 15 min at 25 °C and washing with buffer three times.

Biosensor characterisation. To characterise the biosensor, several features were examined, namely, reproducibility, selectivity towards the antigen, reuse through regeneration, time-stability, and multiplexing. In terms of SERS-based immunoassay, the whole procedure was the same as previously described in section entitled "Regenerated Cellulose Hydrogel for antibody immobilisation.", with the following exceptions: for the selectivity assay, and as a negative control, an irrelevant antigen (*Plasmodium falciparum* His-Rich Protein 2 – *Pf*HRP2, an antigen used for malaria detection assays) was used. For time stability studies, SERS-immunotags and the RCH functionalised with the anti-HRP were kept in phosphate buffer pH 7.4 and PBS 10 mM at 4 °C during assays; the regeneration study was accomplished by immersing the SERS immuno-platform in 100 μL glycine-HCl pH 2.8 for 15 min, and subsequently 1 μL of 1 M Tris-HCl pH 9 was added to restore the original pH of the solution and avoid denaturation of anti-HRP, followed by washing with PBS three times before repeating the incubation step with HRP and the SERS-active SERS-immunotags. A multiplex assay was performed by adding SERS-immunotags with two different Raman reporters (MBA and DTNB) that recognise different antigens, namely, SERS-immunotags with MBA, were formed with monoclonal anti-HRP II that recognises HRP II, and SERS-immunotags with DTNB were formed with anti-HRP that recognises HRP. The SERS-immunotags at 1 nM were let to incubate with the RCH immuno-platform loaded with equivalent amounts of anti-HRP and anti-*Pf*HRP2 and incubated with the respective antigens) as described before in section "Regenerated Cellulose Hydrogel for antibody immobilisation." to allow the formation of the sandwich immunoassay.

SERS-immunotags and regenerated cellulose hydrogel characterisation.

HRP Enzymatic Assay. To determine the viability of anti-HRP antibodies, either in the SERS-immunotags or immobilised in the TO-RCH capture platform, its capacity to bind HRP antigens was tested via an HRP peroxidase enzymatic activity assay. Incubation times were 90 minutes for SERS-immunotags and 30 minutes for the TO-RCH capture platform[16]. Both the SERS-immunotags and the capture platform, before addition of HRP, had non-detectable enzymatic activity. Detection of peroxidase enzymatic activity was based on the Sigma-Aldrich protocol[57]. Measurements were carried out at 25 °C and pH = 5, $Abs_{405\ nm}$; and light path = 1 cm. A 0.001 M potassium phosphate buffer (pH = 5.0) was prepared as a reference sample. The oxidation of a coloured substrate, ABTS (Roche, France) by the enzyme HRP in the presence of hydrogen peroxide (H_2O_2), was followed by measuring the absorbance at 405 nm.

Optical spectroscopies characterisation. All absorption spectra were recorded by a UV-Vis spectrophotometer Cary 50 Bio (Varian®, Agilent, USA) using quartz cells with 1 cm path length (Hellma®), at room temperature. The absorbance at 405 nm for the enzymatic assays performed on the RCH was measured in a multifunctional microplate reader TECAN SPARK 10M (Tecan Trading AG, Switzerland). Dynamic light scattering (DLS) and (zeta) ζ-potential measurements were performed in a SZ-100 Nanopartica series (Horiba, Japan). A 4 mW He–Ne laser (532 nm) was used with a fixed 90° scattering angle. All measurements were carried out at 25 °C. In DLS or ζ-potential, each sample was measured three times and each measurement consisted of 10 or 100 acquisitions, respectively.

Morphological characterisation. SEM observations of the RCH were carried out in a Carl Zeiss AURIGA Crossbeam (FIB-SEM) workstation equipped for EDS measurements (AZtec, Oxford Instruments, Oxford, UK). Cellulose membrane samples were placed directly on the SEM support. AFM analyses used an Asylum Research MFP-3D Standalone AFM system (Oxford Instruments). Samples were immobilised on glass slides, previously treated with a 0.01% w/v poly-l-lysine solution. AFM measurements were performed in AC mode with samples immersed in a PBS buffer solution. Silicon AFM probes (Olympus AC240TS, Olympus Corporation, Japan; k = 2 N/m, f_0 = 70 kHz) were used for AFM topographs.

Raman and SERS Measurements.

Raman measurements were performed in a Renishaw inVia Qontor micro-Raman spectrometer equipped with an air-cooled charge-coupled device (CCD) as detector and a He–Ne laser operating at 32 mW of 632.81 nm laser excitation. For the SERS-immunotags in solution (300 μL), and the final immunoassay was performed on the membrane placed onto a microscope slide, the laser beam was focused with 5× (n.a. 0.12) and long-distance 50× (n.a. 0.5) respectively. An integration time of 10 scans of 20 s each was used for all SERS-immunotags measurements. The intensity of the incident laser was 3.2 mW. Raman images of sandwich immunocomplexes on the RCH were obtained using a Raman point mapping method (scan of 21×21 μm, step of 1 μm). Triplicates were taken of all spectra making a total of 1233 points (pixels) *per* sample. Between different Raman sessions, the spectrograph was calibrated using the Raman line at 520.7 cm^{-1} of an internal Si wafer. All SERS spectra were recorded at room temperature.

All raw data were collected digitally with Wire 5.0 software. Noise reduction, available on the software, was used to estimate and remove the noise through principal component analysis (PCA).

Baseline correction using a polynomial fitting (11th order) was then performed, taking care to ensure minimal alteration of raw data.

Statistical analysis. For AGE, enzymatic assays and SERS-activity assays, results were presented as mean ± standard-deviation from at least three independent experiments run in triplicates. Normality of the data distribution was assessed firstly by the Kolmogorov-Smirnov[58] and then by Shapiro-Wilk[59] test for increased statistical power. The conjugation efficiency and antigen detection in AGE assays, and covalent and electrostatic methods in enzymatic assays were statistically compared using two-sample Student t-test, acquiring the p-value accordingly with Welch correction[60]. To perform a statistical group comparison tests, one-way analysis of variance (ANOVA)[61] followed by the Tukey's multiple comparison test were applied[62]. Outliers were identified by Grubbs test[63]. Significance was considered when *p-values* ≤ 0.05. Nonparametric analysis of variance (Kruskal-Wallis test[58]) was performed on the CLS score of individual immunoassay samples across all populations to test the statistical difference between groups.

Author Contributions

M.J. conceptualisation, formal analysis, and writing – original draft. I.C. produced the hydrogel and T.R.C. supported the AFM characterisation, and both assisted on data analysis and provided support to manuscript preparation. H.A., R.F. and H.J.B. supervision the work, and together with M.P.d.A and E.P., Writing – review & editing until its final form. H.A., R.F. and E.P., and, R.M. and E.F provided the funding, fabrication and characterisation facilities and reviewed the final version of the manuscript. The manuscript was written through contributions of all authors. All authors have given approval to the final version of the manuscript.

Conflicts of interest

There are no conflicts to declare.

Acknowledgements

This work is funded by FEDER funds through the COMPETE 2020 Programme and National Funds through the FCT—Fundação para a Ciência e a Tecnologia, I.P., under the scope of the project UIDB/50025/2020.

This work also received funding from the European Community's H2020 program under grant agreement No. 716510 (ERC-2016-STG TREND), No. 640598 (ERC-StG-2014, NEWFUN), and No. 685758 (1D-Neon). This work was supported by the Applied Molecular Biosciences Unit - UCIBIO and Associate Laboratory for Green Chemistry - LAQV which are financed by Portugal national funds from FCT/MCTES (UIDB/04378/2020 and UIDB/50006/2020), and grant PTDC/NAN-MAT/30589/2017, and fellowships SFRH/BD/126409/2016 and SFRH/BD/132057/2017 from the FCT/MCTES and MIT Portugal PhD Program (to I.C. and M.J.O., respectively). Professor César Laia (LAQV-REQUIMTE, Faculdade de Ciências e Tecnologia, Universidade NOVA de Lisboa, Portugal), is acknowledged for the use of DLS equipment. Professor Ludwig Krippahl (NOVA LINCS, Faculdade de Ciências e Tecnologia, Universidade NOVA de Lisboa, Portugal), is acknowledged for developing the gel analysis application eReuss. M.J.O. acknowledges PhD Rocío Palomares Jurado for visualisation/data presentation support and continued interest in the project. M.J.O. acknowledges MSc David Peitinho for help and advice in Python script. BSc Diego Wiechers de Carvalho is acknowledged for purifying the recombinant *Plasmodium falciparum* histidine-rich protein 2 sample and PhD Daniela Gomes for providing SEM images.

Notes and references

1 P. Ranjan, V. Thomas and P. Kumar, *J. Mater. Chem. B*, , DOI:10.1039/D1TB00071C.

2 L.-K. Lin and L. A. Stanciu, *Sensors Actuators B Chem.*, 2018, **276**, 222–229.

3 C. Li, Y. Liu, X. Zhou and Y. Wang, *J. Mater. Chem. B*, 2020, **8**, 3582–3589.

4 Z. Cheng, N. Choi, R. Wang, S. Lee, K. C. Moon, S. Y. Yoon, L. Chen and J. Choo, *ACS Nano*, 2017, **11**, 4926–4933.

5 G. Li, N. Zhu, J. Zhou, K. Kang, X. Zhou, B. Ying, Q. Yi and Y. Wu, *J. Mater. Chem. B*, 2021, **9**, 2709–2716.

6 A. Kamińska, T. Szymborski, E. Witkowska, E. Kijeńska-Gawrońska, W. Świeszkowski, K. Niciński, J. Trzcińska-Danielewicz and A. Girstun, *Nanomaterials*, , DOI:10.3390/nano9030366.

7 S. Mabbott, S. C. Fernandes, M. Schechinger, G. L. Cote, K. Faulds, C. R. Mace and D. Graham, *Analyst*, 2020, **145**, 983–991.

8 Z. Wang, S. Zong, L. Wu, D. Zhu and Y. Cui, *Chem. Rev.*, 2017, **117**, 7910–7963.

9 D. Wild, J. Rhys and C. Sheehan, Eds., *The Immunoassay Handbook*, Elsevier, Oxford, UK, 4th edn., 2013.

10 A. Kamińska, K. Winkler, A. Kowalska, E. Witkowska, T. Szymborski, A. Janeczek and J. Waluk, *Sci. Rep.*, 2017, **7**, 10656.

11 M. Arabi, A. Ostovan, Z. Zhang, Y. Wang, R. Mei, L. Fu, X. Wang, J. Ma and L. Chen, *Biosens. Bioelectron.*, 2021, **174**, 112825.

12 K. J. Land, D. I. Boeras, X. S. Chen, A. R. Ramsay and R. W. Peeling, *Nat. Microbiol.*, 2019, **4**, 46–54.

13 J. Langer, D. Jimenez de Aberasturi, J. Aizpurua, R. A. Alvarez-Puebla, B. Auguié, J. J. Baumberg, G. C. Bazan, S. E. J. Bell, A. Boisen, A. G. Brolo, J. Choo, D. Cialla-May, V. Deckert, L. Fabris, K. Faulds, F. J. García de Abajo, R. Goodacre, D. Graham, A. J. Haes, C. L. Haynes, C. Huck, T. Itoh, M. Käll, J. Kneipp, N. A. Kotov, H. Kuang, E. C. Le Ru, H. K. Lee, J.-F. Li, X. Y. Ling, S. A. Maier, T. Mayerhöfer, M. Moskovits, K. Murakoshi, J.-M. Nam, S. Nie, Y. Ozaki, I. Pastoriza-Santos, J. Perez-Juste, J. Popp, A. Pucci, S. Reich, B. Ren, G. C. Schatz, T. Shegai, S. Schlücker, L.-L. Tay, K. G. Thomas, Z.-Q. Tian, R. P. Van Duyne, T. Vo-Dinh, Y. Wang, K. A. Willets, C. Xu, H. Xu, Y. Xu, Y. S. Yamamoto, B. Zhao and L. M. Liz-Marzán, *ACS Nano*, 2020, **14**, 28–117.

14 M. J. Oliveira, M. P. de Almeida, D. Nunes, E. Fortunato, R.

Martins, E. Pereira, H. J. Byrne, H. Águas and R. Franco, *Nanomaterials*, 2019, **9**, 1561.

15 M. A. S. Cavadas, M. P. Monopoli, C. S. e Cunha, M. Prudêncio, E. Pereira, I. Lynch, K. A. Dawson and R. Franco, *Part. Part. Syst. Charact.*, 2016, **33**, 906–915.

16 S. Puertas, P. Batalla, M. Moros, E. Polo, P. del Pino, J. M. Guisán, V. Grazú and J. M. de la Fuente, *ACS Nano*, 2011, **5**, 4521–4528.

17 K. Tripathi and J. D. Driskell, *ACS Omega*, 2018, **3**, 8253–8259.

18 M. J. Oliveira, P. Quaresma, M. Peixoto de Almeida, A. Araújo, E. Pereira, E. Fortunato, R. Martins, R. Franco and H. Águas, *Sci. Rep.*, 2017, **7**, 2480.

19 Z. Huang, A. Zhang, Q. Zhang and D. Cui, *J. Mater. Chem. B*, 2019, **7**, 3755–3774.

20 Z. Tan, Y. Zhang, B. D. Thackray and J. Ye, *J. Appl. Phys.*, 2019, **125**, 173101.

21 L. M. Fullwood, D. Griffiths, K. Ashton, T. Dawson, R. W. Lea, C. Davis, F. Bonnier, H. J. Byrne and M. J. Baker, *Analyst*, 2014, **139**, 446–454.

22 A. T. Vicente, A. Araújo, M. J. Mendes, D. Nunes, M. J. Oliveira, O. Sanchez-Sobrado, M. P. Ferreira, H. Águas, E. Fortunato and R. Martins, *J. Mater. Chem. C*, 2018, **6**, 3143–3181.

23 S. Arola, T. Tammelin, H. Setälä, A. Tullila and M. B. Linder, *Biomacromolecules*, 2012, **13**, 594–603.

24 S. Shin and J. Hyun, *ACS Appl. Mater. Interfaces*, 2017, **9**, 26438–26446.

25 B. Ying, S. Park, L. Chen, X. Dong, E. W. K. Young and X. Liu, *Lab Chip*, 2020, **20**, 3322–3333.

26 M. E. Keating, H. Nawaz, F. Bonnier and H. J. Byrne, *Analyst*, 2015, **140**, 2482–2492.

27 C. D. L. de Albuquerque, R. G. Sobral-Filho, R. J. Poppi and A. G. Brolo, *Anal. Chem.*, 2018, **90**, 1248–1254.

28 Z. Tan, Y. Zhang, B. D. Thackray and J. Ye, *J. Appl. Phys.*, 2019, **125**, 173101.

29 H. J. Byrne, P. Knief, M. E. Keating and F. Bonnier, *Chem. Soc. Rev.*, 2016, **45**, 1865–1878.

30 H. Yuan, C. G. Khoury, H. Hwang, C. M. Wilson, G. A. Grant and T. Vo-Dinh, *Nanotechnology*, 2012, **23**, 075102.

31 D. Bartczak and A. G. Kanaras, *Langmuir*, 2011, **27**, 10119–10123.

32 I. Cunha, R. Barras, P. Grey, D. Gaspar, E. Fortunato, R. Martins and L. Pereira, *Adv. Funct. Mater.*, 2017, **27**, 1606755.

33 G. T. Hermanson, *Bioconjugate Techniques: Third Edition*, Elsevier, London, Third., 2013.

34 C. M. Silveira, R. Zumpano, M. Moreira, M. P. de Almeida, M. J. Oliveira, M. Bento, C. Montez, I. Paixão, R. Franco, E. Pereira and M. G. Almeida, *ChemElectroChem*, 2019, **6**, 4696–4703.

35 M. Peixoto de Almeida, P. Quaresma, S. Sousa, C. Couto, I. Gomes, L. Krippahl, R. Franco and E. Pereira, *Phys. Chem. Chem. Phys.*, 2018, **20**, 16761–16769.

36 J. Guo, F. Zeng, J. Guo and X. Ma, *J. Mater. Sci. Technol.*, 2020, **37**, 96–103.

37 A. Isogai, T. Saito and H. Fukuzumi, *Nanoscale*, 2011, **3**, 71–85.

38 J. Łojewska, P. Miśkowiec, T. Łojewski and L. M. Proniewicz, *Polym. Degrad. Stab.*, 2005, **88**, 512–520.

39 H. Orelma, I. Filpponen, L.-S. Johansson, M. Österberg, O. J. Rojas and J. Laine, *Biointerphases*, 2012, **7**, 61.

40 C. Bustamante and D. Keller, *Phys. Today*, 1995, **48**, 32–38.

41 M. E. Keating, F. Bonnier and H. J. Byrne, *Analyst*, 2012, **137**, 5792.

42 M. Nič, J. Jirát, B. Košata, A. Jenkins and A. McNaught, Eds., *IUPAC Compendium of Chemical Terminology*, IUPAC, Research Triagle Park, NC, 2009.

43 R. Frimpong, W. Jang, J. H. Kim and J. D. Driskell, *Talanta*, 2021, **223**, 121739.

44 D. Lu, M. Ran, Y. Liu, J. Xia, L. Bi and X. Cao, *Anal. Bioanal. Chem.*, 2020, **412**, 7099–7112.

45 J. Huang, X. Zhang, S. Liu, Q. Lin, X. He, X. Xing and W. Lian, *J. Appl. Electrochem.*, 2011, **41**, 1323–1328.

46 L. Wu, X. Lu, K. Niu, Dhanjai and J. Chen, *Biosens. Bioelectron.*, 2020, **165**, 112407.

47 A. Kim, C. R. Li, C. F. Jin, K. W. Lee, S. H. Lee, K. J. Shon, N. G. Park, D. K. Kim, S. W. Kang, Y. B. Shim and J. S. Park, *Chemosphere*, 2007, **68**, 1204–1209.

48 I. Gomes, A. Reis, E. Fortunato, M. Prudêncio and R. Franco, *An. Inst. Hig. e Med. Trop.*, 2015, **14**, 21–30.

49 Y. Li, Q. Chen, X. Xu, Y. Jin, Y. Wang, L. Zhang, W. Yang, L. He, X. Feng and Y. Chen, *Sensors Actuators, B Chem.*, 2018, **266**, 115–123.

50 J. A. Goode, J. V. H. Rushworth and P. A. Millner, *Langmuir*, 2015, **31**, 6267–6276.

51 W. W. Yu and I. M. White, *Analyst*, 2013, **138**, 1020–1025.

52 P. K. Smith, R. I. Krohn, G. T. Hermanson, A. K. Mallia, F. H. Gartner, M. D. Provenzano, E. K. Fujimoto, N. M. Goeke, B. J. Olson and D. C. Klenk, *Anal. Biochem.*, 1985, **150**, 76–85.

53 I. Ojea-Jiménez, N. G. Bastús and V. Puntes, *J. Phys. Chem. C*, 2011, **115**, 15752–15757.

54 Q. Yang, H. Fukuzumi, T. Saito, A. Isogai and L. Zhang, *Biomacromolecules*, 2011, **12**, 2766–2771.

55 M. He, Y. Zhao, J. Duan, Z. Wang, Y. Chen and L. Zhang, *ACS Appl. Mater. Interfaces*, 2014, **6**, 1872–1878.

56 C. K. Dixit, S. K. Vashist, B. D. MacCraith and R. O'Kennedy, *Nat. Protoc.*, 2011, **6**, 439–445.

57 Sigma-Aldrich, Enzymatic Assay of Peroxidase (EC 1.11.1.7) 2,2'-Azino-bis(3-Ethylbenzthiazoline-6-Sulfonic Acid) as a Substrate, https://www.sigmaaldrich.com/technical-documents/protocols/biology/enzymatic-assay-of-peroxidase-abts-as-substrate.html, (accessed 29 July 2019).

58 D. Sheskin, *Handbook of Parametric and Nonparametric Statistical Procedures*, Taylor & Francis, Boca Raton, Florida, 5th edn., 2011.

59 S. S. Shapiro and M. B. Wilk, *Biometrika*, 1965, **52**, 591.

60 B. L. Welch, *Biometrika*, 1947, **34**, 28.

61 P. T. Munroe, *Blackwell Encycl. Sociol.*, , DOI:10.1002/9781405165518.wbeosa055.pub2.

62 J. W. Tukey, *Stat. Sci.*, 1991, **6**, 100–116.

63 F. E. Grubbs, *Ann. Math. Stat.*, 1950, **21**, 27–58.